

Article

Experimental Study on the Short-Term Uniaxial Creep Characteristics of Sandstone-Coal Composite Samples

Dawei Yin ¹, Feng Wang ^{1,*}, Jicheng Zhang ¹, Faxin Li ¹, Chun Zhu ² and Fan Feng ¹

¹ State Key Laboratory of Mine Disaster Prevention and Control, Shandong University of Science and Technology, Qingdao 266590, China; yindawei@sdust.edu.cn (D.Y.); 202081010096@sdust.edu.cn (J.Z.); lifaxin@sdust.edu.cn (F.L.); fengfan0213@sdust.edu.cn (F.F.)

² School of Earth Sciences and Engineering, Hohai University, Nanjing 210098, China; zhu.chun@hhu.edu.cn

* Correspondence: wangfeng@sdust.edu.cn; Tel.: +86-137-8985-9661

Abstract: In this investigation, the uniaxial short-term creep tests with multi-step loading were conducted on the sandstone-coal composite samples, and the characteristics of creep strength, creep deformation, acoustic emission (AE), and creep failure of composite samples were studied, respectively. The creep strength of the composite sample decreased with the stress-level duration, which was mainly determined by the coal and influenced by the interactions with the sandstone. The creep deformation and damage of sandstone weakened the deformation and damage accumulation within the coal, resulting in the larger strength for the composite sample compared with the pure coal sample. The axial creep strain of composite sample generally increased with the stress-level or the stress-level duration under same conditions. The AE characteristics of composite sample were related to the creep strain rate, the stress level, the stress level duration, and the local failure or fracture during creep loading. The micro or macro failure and fracture within the composite sample caused the rise in the axial creep strains and the frequency and intensity of AE signals, especially the macro failure and fracture. The creep failures of composite samples mainly occurred within the coal with the splitting ejection failure accompanied by the local shear failure, and no obvious failures were found within the sandstone. The coal in the composite sample became more broken with the stress-level duration.

Keywords: sandstone-coal composite samples; creep strength; creep deformation; acoustic emission characteristics; creep failure; short-term uniaxial creep loading



Citation: Yin, D.; Wang, F.; Zhang, J.; Li, F.; Zhu, C.; Feng, F. Experimental Study on the Short-Term Uniaxial Creep Characteristics of Sandstone-Coal Composite Samples. *Minerals* **2021**, *11*, 1398. <https://doi.org/10.3390/min11121398>

Academic Editor: Gianvito Scaringi

Received: 15 October 2021

Accepted: 8 December 2021

Published: 10 December 2021

Publisher's Note: MDPI stays neutral with regard to jurisdictional claims in published maps and institutional affiliations.



Copyright: © 2021 by the authors. Licensee MDPI, Basel, Switzerland. This article is an open access article distributed under the terms and conditions of the Creative Commons Attribution (CC BY) license (<https://creativecommons.org/licenses/by/4.0/>).

1. Introduction

Coal is the foundation of energy, and the major resource in China, which effectively promotes the development of economy and society nationally [1–3]. In order to ensure the safety, high efficiency and green mining of coal resources in China, different types and functions of coal pillars have been left around the mining area [4–8], such as the strip coal pillar, the waterproof coal pillar, the section coal pillar, etc. A considerable number of left coal pillars, as the permanent coal pillars, bear loads for a long time to support the overlying strata and to control the surface subsidence or collapse [9–14]. The long-term stability of these coal pillars determines the safety and stability of overlying strata, surface buildings and ecological environment, etc. And their failure and instability can induce the overlying strata caving and surface collapsing in China [7], for instance, the failure and instability of left coal pillars in the 402 panel of Majiliang Coal Mine (Figure 1a) caused the formation of an oval surface collapse area with about 79,103 m²; the failure and instability of left coal pillars in the 404 panel of Wajinwan Coal Mine (Figure 1b) induced the formation of an surface collapse area with about 163,000 m², and resulted in 18 deaths and 19 injuries. Therefore, it is important to investigate the long-term stability of these left coal pillars.

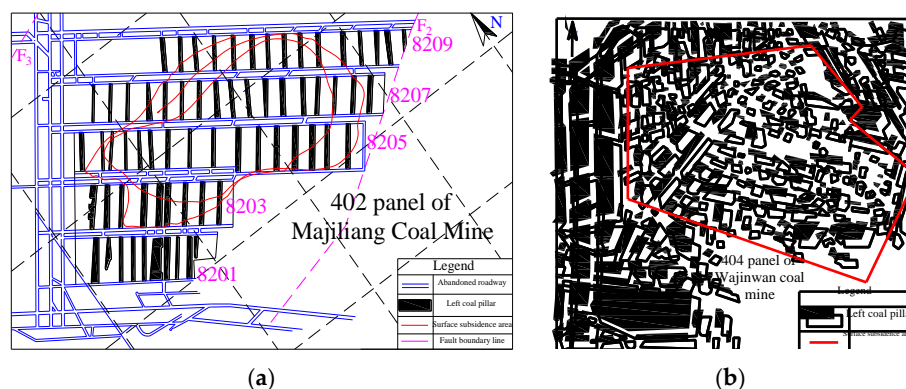


Figure 1. Surface collapsing induced by the failure and instability of left coal pillars in China [4]: (a) Surface collapsing induced by the failure and instability of left coal pillars in 402 panel of Majiliang Coal Mine; (b) Surface collapsing induced by the failure and instability of left coal pillars in 404 panel of Wajinwan Coal Mine.

Many investigations have achieved that the long-term bearing failure and instability of the coal pillar are a mechanical behavior gradually developing from the edge to its interior [4,7–12]. These are not only related to the properties of coal pillar itself, but also affected by the composite structure consisting of coal pillar and surrounding rock layers [6–36]. In other words, the instability of coal pillar is the result of the overall failure and instability of composite structure under overlying strata loads. Therefore, the long-term bearing characteristics and failure mechanisms of coal pillar should be investigated considering the composite structure. Generally, these composite structures were simplified to the rock–coal, coal–rock, and rock–coal–rock composite samples with a bonded or frictional interface to study their mechanical behaviors in previous experimental and numerical simulation investigations [12–36]. These studies focused on the effects of the height ratio of coal to rock [12,22,31–33], the interface between rock and coal [11–14,19], the composite model [36], the loading conditions (uniaxial loading, triaxial loading, cyclic loading and unloading, and true triaxial loading) [14,21,24,25,27,34,35], the defects within the coal or rock, and the mechanical properties (strength, stiffness, lithology, etc.) of rock or coal [19,20,26] on the strength, deformation, energy evolution, electromagnetic radiation characteristics [28,29], acoustic emission (AE) characteristics, and failure properties of composite samples. These above achievements are of great significance to understand mechanical characteristics of the composite structure consisting of coal pillar and surrounding rock layers.

The creep tests on rock or coal samples are very important methods to understand the long-term bearing characteristics and failure mechanisms of coal or rock mass [37–46], and these investigations mainly focused on pure coal or rock samples. Fatemeh and Mark [37] carried out the creep experiments on clay- and carbonate-rich shale samples with short-term (4 h) and long-term (4 weeks) periods, respectively, the results showed that the shale samples follow the same creep trend through time, regardless of the loading history. Cao et al. [38] proposed a nonlinear damage creep constitutive model describing the creep deformation of soft rock. Maranini and Brignoli [39] investigated the creep behavior of a porous chalk, named Pietra Liccese, and proposed an elasto-viscoplastic model describing the slow irreversible deformation in time of the rock surrounding underground openings. Yang et al. [40] analyzed the influences of confining pressure and pore pressure on short-term mechanical behavior of red sandstone samples, and the creep contribution to rock deformation increased with the pore pressure, and the samples showed significant time-dependent effect at higher deviatoric stresses. Yang et al. [41] studied the evolution characteristics of deformation field for red sandstone during the creep loading using the digital image correlation technique. Zong et al. [42] discussed the effects of the confining pressure and damage on short-term mechanical behavior of fractured sandstone with different degrees of damage. Yang et al. [43] and Cao et al. [44] analyzed the AE characteristics of coal samples under creep loading, respectively. Chen et al. [45] and Wu et al. [46] proposed

the creep model for coal samples and the nonlinear creep damage model for salt rock, respectively. These above achievements are of great significance to understand the creep behavior of engineering coal or rock mass

However, the creep investigations that focused on the rock–coal, coal–rock, and rock–coal–rock composite samples have been scant. The creep tests can be classified as long-term creep tests and short-term creep tests based on the stress level duration, but there are no definite time requirements for this classification. Short-term creep tests typically have a stress level duration of several hours or days, whereas long-term creep tests can have a stress level duration of several weeks or even years. A large number of investigations have shown that the creep parameters measured by the short-term creep tests can give a reasonably understanding of the long-term behavior of the rock and help avoid time-consuming [37,40,44–47]. In this investigation, we conducted the short-term uniaxial multi-step loading creep tests with different stress-level durations on the sandstone–coal composite samples, and the characteristics of creep strength, creep deformation, AE, and creep failure of composite samples were studied, respectively.

2. Experimental Procedure

2.1. Sample Preparation

In this investigation, the rock in the composite sample was the sandstone. Sandstone and coal blocks were taken from the Daizhuang Coal Mine in Jining City of China. The sandstone was from the immediate roof. The heights of both the rock and coal layers were 50 mm in the composite samples with a diameter of 50 mm and a height of 100 mm. Firstly, the sandstone and coal blocks were drilled into the cylindrical samples with a diameter of 50 mm. Then, the cylindrical samples were cut into 50 mm height by a stone-sawing machine. Then both ends of cylinder samples were flattened, and smoothed to meet the experimental requirements, respectively, by a stone grinding machine. Finally, the cylinder coal and sandstone samples with a diameter of 50 mm and a height of 50 mm were bonded with superglue to make the 100 mm high sandstone–coal composite samples. Nine composite samples were well prepared, three of which (Figure 2a) were used to test their mechanical properties under uniaxial loading, and the other composite samples (Figure 2b) were subjected to the short-term uniaxial creep tests.

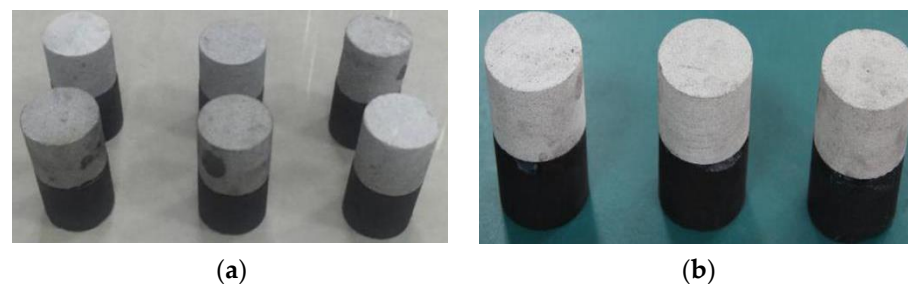


Figure 2. Sandstone–coal composite samples: (a) Sandstone–coal composite samples for creep tests; (b) Sandstone–coal composite samples for uniaxial compression tests.

2.2. Test System

The testing system for short-term uniaxial creep with multi-step loading on sandstone–coal composite samples is shown in Figure 3, including a loading system, an AE monitoring system, and a digital video camera (DVC) (Sony, Tokyo, Japan). During each test, they were synchronized to have the same time stamp in order to facilitate analyses of test results.

An AG-X250 servo-controlled testing system (Shimadzu, Kyoto, Japan) was used to perform the short-term uniaxial creep tests on the composite samples [12–14,20]. The AE event was selected to analyze the AE characteristics of composite samples during creep loading, which was monitored using a PCI-2 AE system (MISTRAS, Princeton, NJ, USA) by MISTRAS. The AE sensor was a R3 α with a diameter of 19 mm and a height of 22 mm.

Its resonant frequency was 29 kHz, and the range of frequency was 20–180 kHz. The main amplifier gain, threshold, floating threshold, and sampling frequency of the AE monitoring system were 40 dB, 45 dB, 6 dB, and 1 MHz, respectively. The Vaseline was applied between the sample surface and AE sensor in order to improve the coupling conditions. One AE sensor was fixed to the sandstone surface with the adhesive tape. Before the tests, the AE sensor was subjected to a pencil-lead breaking test proposed by ASTM (American Society for Testing and Materials) to ensure that the amplitude measured was above 90 dB. A SONY portable DVC was used to capture the stage points in progressive failure processes of composite samples during creep loading. Generally, the laboratory temperature affected the creep characteristics of samples, and the creep deformation increased with the decrease of the laboratory temperature. The laboratory temperature was set to 24 °C to reduce the temperature effects during creep tests by running the air conditioning.

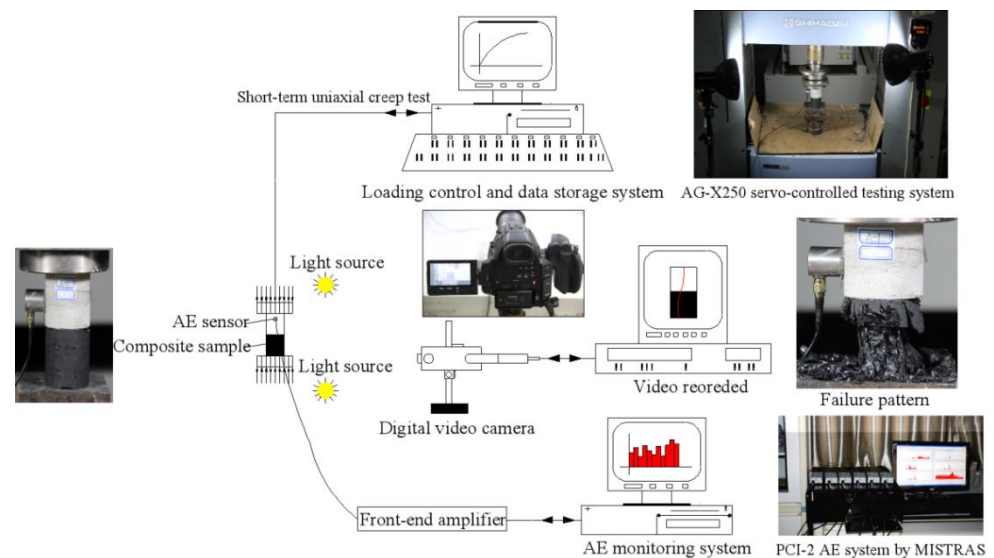


Figure 3. Testing system for short-term uniaxial creep on sandstone-coal composite samples (revised from Yin et al. [20]).

2.3. Test Scheme

Before the short-term uniaxial creep testing, uniaxial compressive tests were carried out on three sandstone-coal composite samples (labeled as RC-1, RC-2 and RC-3) to obtain their basic mechanical properties, using the AG-X250 servo-controlled testing system under the displacement-controlled mode at a loading rate of 0.01 mm/s. Figure 4 shows uniaxial stress-strain curves of composite samples; their uniaxial mechanical properties are listed in Table 1.

Table 1. Mechanical properties of sandstone-coal composite samples under uniaxial loading.

Sample Type	Sample No.	Uniaxial Compressive Strength (UCS)/MPa	Peak Strain	Elastic Modulus/GPa (at 40–60% of Peak Stress)
Sandstone-coal composite sample	RC-1	14.36	0.00985	2.11
	RC-2	14.08	0.00775	2.52
	RC-3	13.99	0.00853	2.44
	Average	14.14	0.00871	2.36

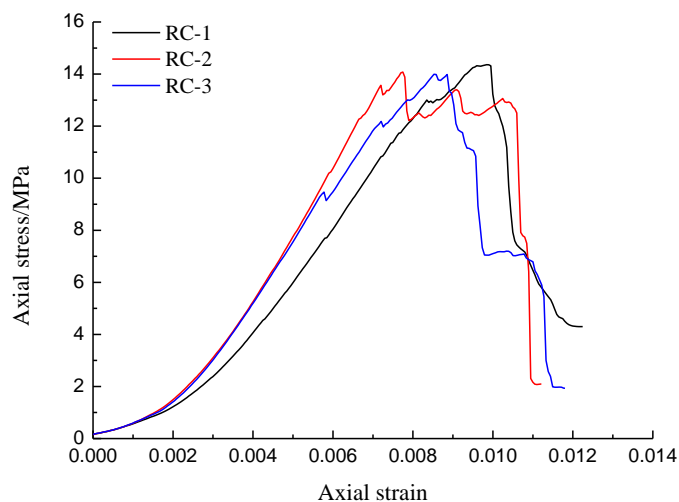


Figure 4. Uniaxial stress-strain curves of sandstone-coal composite samples.

In Table 1, the average UCS, peak strain and elastic modulus of sandstone-coal composite samples were 14.14 MPa, 0.00871, and 2.36 GPa, respectively. Generally, the creep tests were carried out by methods of single-stage loading, multi-stage loading, and multi-stage loading and unloading in previous investigations on the creep characteristics of pure coal or rock samples [37–46]. In this investigation, the short-term uniaxial creep tests with multi-stage loading were conducted on sandstone-coal composite samples. According to the results of uniaxial compression tests, the axial stresses of 50%, 60%, 70%, 80%, 85%, 90%, 95%, of the average UCS (σ) were gradually applied on composite samples until they underwent the failure, as shown in Figure 5. The corresponding axial stresses were 7.07 MPa, 8.48 MPa, 9.90 MPa, 11.31 MPa, 12.02 MPa, 12.73 MPa, 13.44 MPa, , respectively. The stress level durations (S) were set to 2 h and 6 h, respectively. The axial stress was firstly applied on the composite samples from 0 kN to the 13.88 kN (the first stress level) at a loading rate of 0.005 kN/s, and the loading rate between two adjacent stress levels was also set to 0.005 kN/s. The test data acquisition interval between two adjacent stress level was set to 0.5 s, and the data acquisition interval during each stress level was set to 1 s.

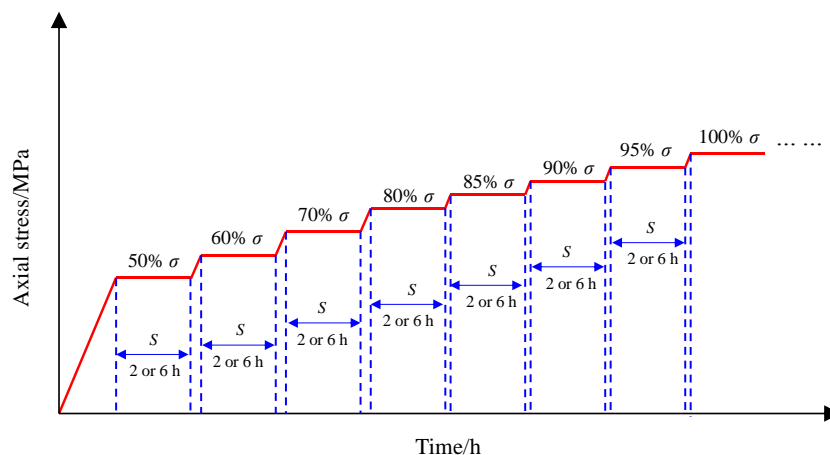


Figure 5. Creep test scheme for sandstone-coal composite samples.

3. Creep Strength Characteristics of Composite Samples

3.1. Creep Strengths of Composite Samples

The creep strength σ_{rc} of the composite sample was given in Equation (1),

$$\sigma_{rc} = \sigma_{n-1} + (\sigma_n - \sigma_{n-1}) \frac{t}{S} \tag{1}$$

where, σ_n was the stress level leading to failure; σ_{n-1} was the stress level before σ_n , t was the loading duration at the stress level of σ_n ; S was the horizontal loading duration of each level of stress.

Table 2 shows the values of σ_{rc} , σ_n , σ_{n-1} , t and creep coefficients (ratio of σ_{rc} and σ) of composite samples. Among them, the stress level durations corresponding to Groups A and B composite samples were 2 h and 6 h, respectively. The values of σ_{rc} and creep coefficients for composite samples were compared in Figure 6a,b, respectively.

Table 2. σ_n , σ_{n-1} , t and creep coefficients of sandstone-coal composite samples.

Sample Type	Sample No.	S/h	σ_n /MPa	σ_{n-1} /MPa	t/s	σ_{rc} /MPa	Creep Coefficient
Sandstone-coal composite sample	A-1	2	13.44	12.73	380	12.77	90.24%
	A-2		14.14	13.44	782	13.52	95.47%
	A-3		13.44	12.73	1035	12.83	90.88%
	Average value		—	—	—	13.05	92.20%
	B-1	6	13.44	12.73	2700	12.82	90.66%
	B-2		12.02	11.31	3435	11.42	80.76%
	B-3		11.31	9.90	455	9.93	70.23%
	Average value		—	—	—	11.39	80.55%

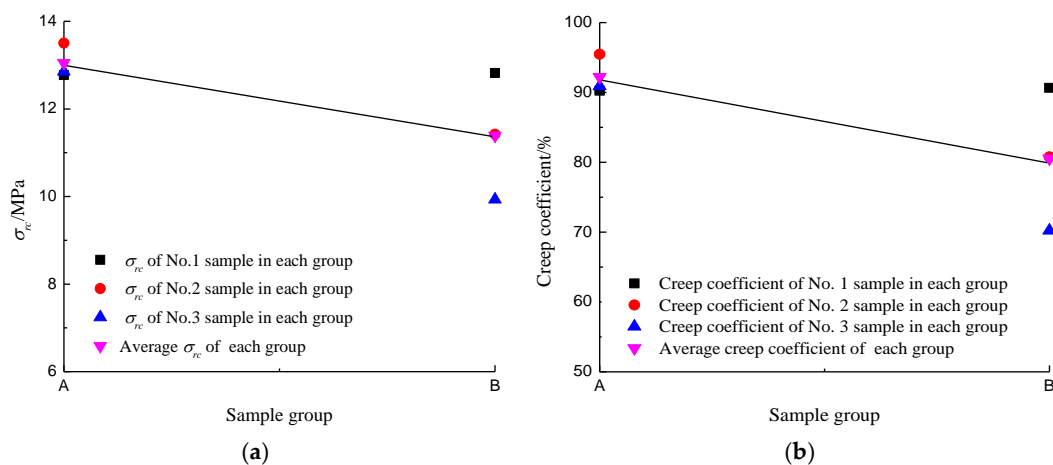


Figure 6. Comparisons of σ_{rc} and creep coefficients for composite samples: (a) σ_{rc} comparison of composite samples; (b) Creep coefficient comparison of composite samples.

In Table 2 and Figure 6, σ_{rc} and creep coefficients of composite samples varied with the stress level duration. The average σ_{rc} of Group A composite samples was 13.05 MPa with an average creep coefficient of 92.20%; whereas the average σ_{rc} of Group B composite samples was 11.39 MPa, and their average creep coefficient was 80.55%. These illustrated that as S increased from 2 h to 6 h, σ_{rc} and creep coefficients of composite samples gradually decreased, which were consistent with previous investigations on creep characteristics of pure coal or rock samples. Compared with Group A composite samples, both average σ_{rc} and creep coefficient of Group B composite samples decreased by 12.45%.

3.2. Analyses on Creep Strength Characteristics of Composite Samples

The failure properties could well reflect the strength characteristics of the sample under loading. After the short-term uniaxial creep loading, the failures of composite samples mainly occurred within the coal, and no obvious failures were found in the sandstone (in Section 6). These illustrated that the failure of coal determined the overall instability of the composite sample, i.e., the creep strength of coal played a major in the creep strength of the composite sample. In order to analyze the relationship between creep strengths of pure coal samples and composite samples, the short-term uniaxial creep tests with multi-stage loading were conducted on pure coal samples (labeled as PC-1 and PC-2) with a diameter of 50 mm and a height of 50 mm using the AG-X250 servo-controlled testing system (Figure 7). And the test scheme was same as that of composite samples.



Figure 7. Short-term uniaxial creep tests on pure coal samples.

Figure 8a,b show the creep curves of PC-1 and PC-2 pure coal samples, respectively, and the values of their creep strengths (σ_{pc}), σ_n , σ_{n-1} and t are given in Table 3. In Table 3, the values of σ_{pc} for PC-1 and PC-2 pure coal samples were 12.46 MPa and 11.39 MPa, respectively, which were different from σ_{rc} of composite samples. σ_{pc} and σ_{rc} are compared in Figure 9.

Table 3. σ_n , σ_{n-1} and t and creep coefficients of pure coal samples.

Sample Type	Sample No.	σ_n /MPa	σ_{n-1} /MPa	t /s	σ_{pc} /MPa	T /h
Pure coal sample	PC-1	12.73	12.02	4481	12.46	2
	PC-2	12.02	11.31	2480	11.39	6

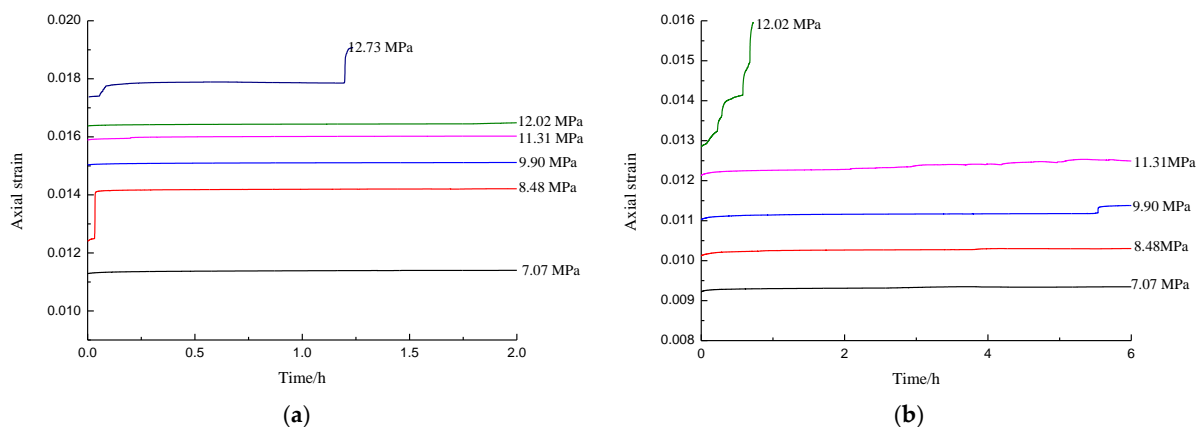


Figure 8. Creep curves of pure coal samples: (a) Creep curve of PC-1 pure coal sample; (b) Creep curve of PC-2 pure coal sample.

For the pure coal sample, under the actions of gradual stress levels, it was incurred creep deformations and damages. When the accumulative creep deformations (damages) reached its creep deformations (damages) limit, pure coal sample would fail. However, the sandstone-coal composite sample was a combined body, under the actions of gradual stress levels, the rock and coal in the composite sample were both incurred creep deformations and damages. The average UCS of sandstone (72.89 MPa) was 4.82 times larger than that of coal (15.11 MPa). The coal in the composite sample would occur creep failure first, inducing the overall instability and failure of the composite sample. While the sandstone was still at the linear elastic stage due to its larger strength. Before the creep failure of coal, the sandstone has had creep deformations occur, consuming some applied mechanical work as strain energy in it. Therefore, under the certain external input energy, the creep deformation and damage in coal of the composite sample was smaller than that in pure coal sample. The creep deformation of sandstone limited the accumulations of creep deformation (damage) in coal, and which would be destroyed at a higher input energy level compared with the pure coal sample. Therefore, the creep strengths of composite samples were larger than that of pure coal samples. In Figure 9a, compared with σ_{pc} of PC-1 pure coal sample, the values of σ_{rc} for A-1, A-2, and A-3 composite samples increased by 2.49%, 8.51%, and 2.97%, respectively. In Figure 9b, compared with the σ_{pc} of PC-2 pure coal sample, the values of σ_{rc} for B-1, and B-2 composite samples increased by 2.49%, 8.51%, and 2.97%, respectively. However, σ_{rc} of B-3 composite sample decreased by 12.82% compared with σ_{pc} of PC-2 pure coal sample. This was mainly because that the initial damages in coal were relatively larger that of B-1, B-2 composite samples and PC-2 pure coal sample.

It is important to point out that the sandstone was at the linear elastic stage when the coal occurred the creep failure. The creep failure of coal could cause the rebound deformation of sandstone, and strain energy in it would release rapidly. Partial strain energy was used to overcome the damping of sandstone to restore its the initial state. The other strain energy exerted work on the coal to promote its further creep failure. This process appeared before the occurrence of main creep fracture in coal.

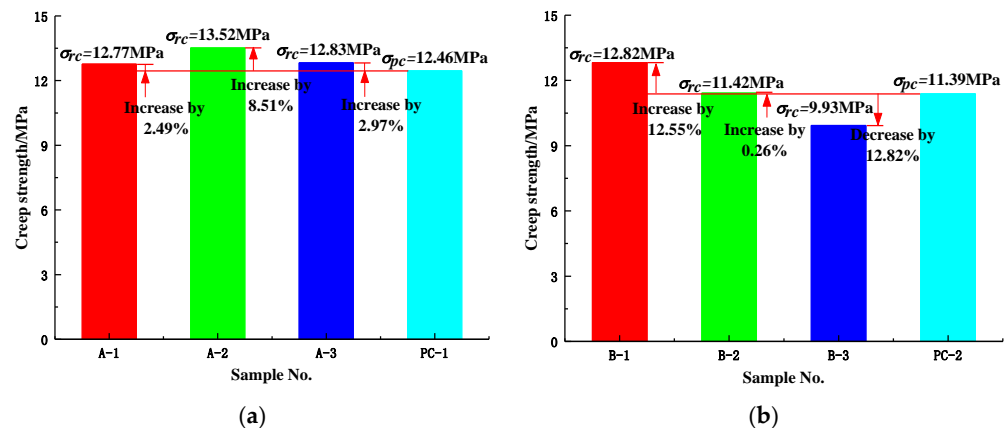


Figure 9. Comparisons of σ_{pc} and σ_{rc} for composite samples and pure coal samples: (a) Comparisons of σ_{pc} and σ_{rc} of Group A composite samples and PC-1 pure coal sample; (b) Comparisons of σ_{pc} and σ_{rc} of Group B composite samples and PC-2 pure coal sample.

4. Creep Deformation Characteristics of Composite Samples

Data acquisition interval in these creep tests was relatively small, and the amount of data was large and dense, which were of great significances to the analysis of creep deformation characteristics of composite samples. Figure 10a,b show creep curves of A-1 and B-3 composite samples, respectively. The axial creep strains of Groups A and B composite samples at different stress levels are compared in Figure 11a,b, respectively.

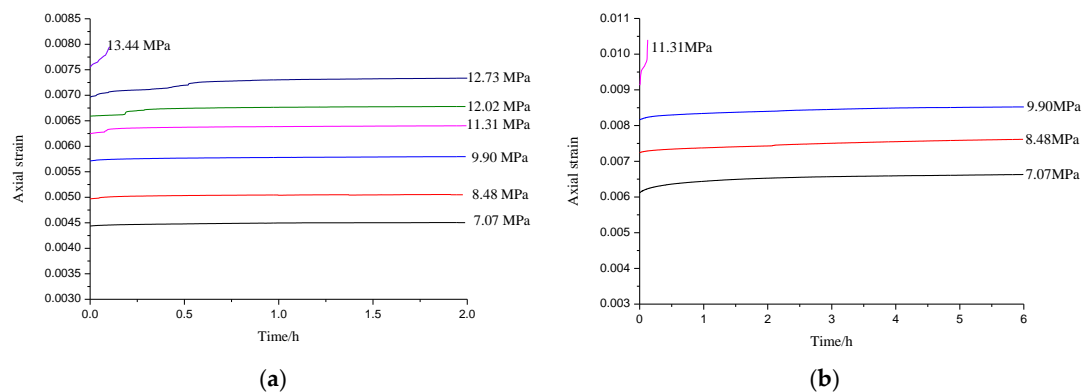


Figure 10. Typical creep curves of sandstone-coal composite samples: (a) Creep curve of A-1 composite sample; (b) Creep curve of B-3 composite sample.

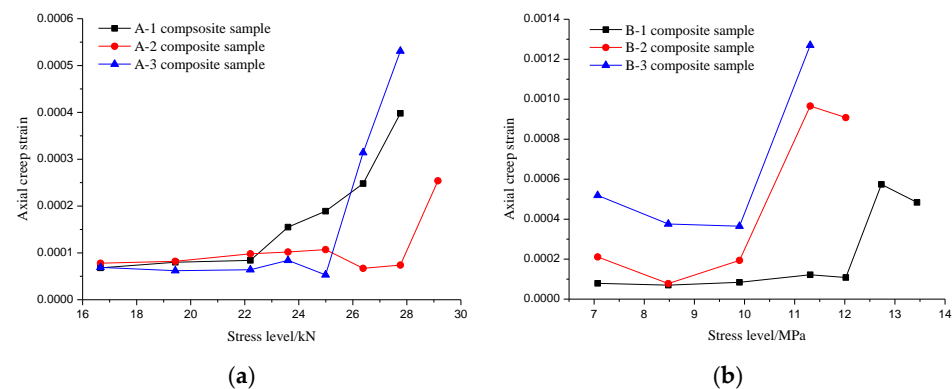


Figure 11. Axial creep strains of sandstone-coal composite samples at different stress levels: (a) Axial creep strains of Group A composite samples; (b) Axial creep strains of Group B composite samples.

In Figure 10, at the beginning of each stress level, the composite sample occurred the instantaneous elastic response, producing the instantaneous elastic deformation. After the stress was stable, the composite sample entered the creep stage, and occurred the creep deformation. The creep deformation rate decreased with the loading time at the deceleration creeping stage, and it tended to be stable finally at the stable creeping stage. At each stress level, the creep curves of composite samples all appeared the deceleration creeping stage and stable creeping stage. Meanwhile, the creep curves of composite samples occurred the unstable creeping stage, and the corresponding creep deformation sharply increased at the last stress level. Then composite samples experienced the creep failure and instability.

In Figure 11, as a whole, the axial creep strain increased with the stress level, and under same stress level, the longer the loading time was, the higher the creep strain was. However, the phenomena of a low stress level with a large axial creep strain, a high stress level with a low axial strain, and a short stress level duration with a great axial creep strain under same stress level, were also found in Figure 11. For example, under the stress level of 11.31 MPa, the axial strain of A-1 composite sample was larger than that of B-1 composite sample. The main reason for these phenomena was that the creep process was a concurrent process of hardening and softening for composite sample at each stress level, which was the comprehensive embodiment of the competition between the hardening and softening. When creep softening was dominant, the corresponding creep strain was relatively large, while when creep hardening was dominant, the corresponding creep strain was relatively small. Meanwhile, before the unstable creeping stage, the axial creep strain-time curve did not increase steady, but occurred the slight or violent local increasing fluctuations, as shown in Figure 12. These also induced the abnormal axial creep strain variation phenomena in Figure 11.

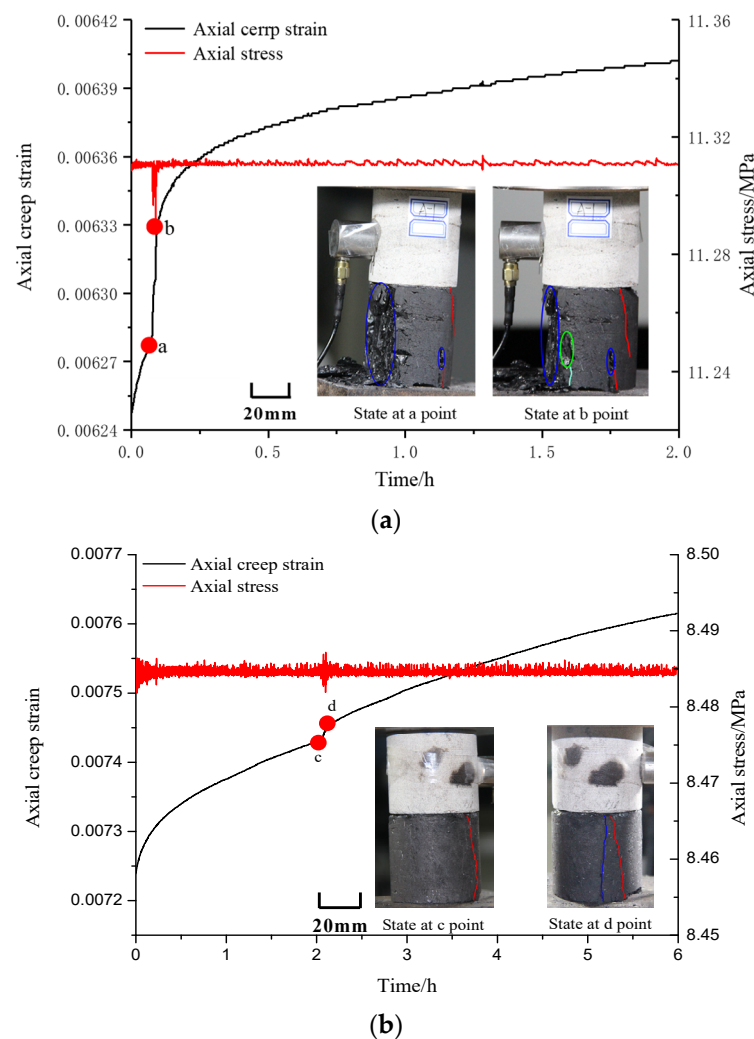


Figure 12. Axial creep strain fluctuations of sandstone-coal composite samples (the scale bar between the sample size in the figure and that of the real sample is 1:4): (a) Axial creep strain fluctuation of A-1 composite sample at the stress level of 11.31 MPa; (b) Axial creep strain fluctuation of B-3 composite sample at the stress level of 8.48 MPa.

In Figure 12a, the A-1 composite sample occurred the splitting ejection failure within coal before a point, and this failure was caused by the loading from the stress level of 8.48 MPa to the stress level of 9.90 MPa, which was analyzed comprehensively in Section 5. From a point to b point, the composite sample experienced the splitting ejection failure within coal around the initial splitting ejection failure zone again, as shown in the green elliptical area of Figure 12a. This process was accompanied with the macro-crack initiation and propagation near the new formed splitting ejection failure zone. These failures induced the linear sudden increase of axial creep strain, and the corresponding axial stress had a sudden drop. The axial creep strain was 0.000050 from a point to b point, which accounted for 32.26% of the whole axial creep strain at the stress level of 11.31 MPa. In Figure 12b, the B-3 composite sample occurred the splitting failure within coal before c point, and an obvious macro-tensile crack was found in coal. This failure was caused by the loading from the initial loading point to the first stress level of 7.07 MPa, as shown in the red line of Figure 12b, which was analyzed comprehensively in Section 5. From c point to d point, the composite sample experienced the splitting failure within coal again, and a blue macro-tensile crack was formed near initial red macro-tensile crack. These failures induced the sudden increase of axial creep strain, and the corresponding axial stress had serious fluctuations. The axial creep strain was 0.000021 from c point to d point, which accounted

for 5.59% of the whole axial creep strain at the stress level of 8.48 MPa. The fluctuation degree of creep axial strain caused by splitting ejection failure was stronger than that by tensile failure.

5. AE Characteristics of Composite Samples

In this investigation, the AE event was selected to analyze AE characteristics of composite samples under short-term uniaxial creep loading. Figures 13 and 14 give the variety curves of AE event and axial strain for A-1 and B-3 composite samples at creep stage for different stress levels, respectively. And a, b, c, d, e, f, g in Figure 13 refer to the stress levels of 7.07 MPa, 8.48 MPa, 9.90 MPa, 11.31 MPa, 12.02 MPa, 12.73 MPa, 13.44 MPa, respectively. And a, b, c, d in Figure 14 refer to the stress levels of 7.07 MPa, 8.48 MPa, 9.90 MPa, 11.31 MPa, respectively. Among them, the a, b, c, and d points in Figures 13 and 14 were same as those in Figure 12, respectively. The AE characteristics of composite samples under short-term uniaxial creep loading were as follows:

(1) At each stress level, the creep strain rate decreased gradually in the deceleration creeping stage, and the intensity and frequency of AE events were remarkably weakened. AE events experienced large fluctuations with peak values at the beginning of this stage. As the time increased, the composite sample entered the stable creeping stage with a constant creep strain rate. The corresponding intensity and frequency of AE events were relatively low and stable. Generally, the deceleration creeping stage and stable creeping stage occurred at a relatively low stress level, and the unstable creeping stage arose at a high stress level. As the composite sample entered the unstable creeping stage, the creep strain rate increased gradually. The composite sample occurred failure and instability. The intensity and frequency of AE events were strengthened again, which exhibited significant fluctuations with more peak values. At the end of this stage, the axial creep strain-time curve rose with a fast creep strain rate, and AE events displayed large fluctuations. The intensity and frequency of AE activities can reflect the creep damage evolution process of composite sample under short-term uniaxial creep loading. Therefore, under same stress level, the creep damage degree at the unstable creeping stage was the most serious, larger than that at the stages of deceleration creeping and stable creeping. The creep damage degree at the stable creeping stage was the lowest.

(2) Under same stress level duration, with the increase of the stress level, the intensity and frequency of AE events at the deceleration creeping stage and stable creeping stage were enhanced. These illustrated that the creep damage degree of the composite sample increased with the stress level. Until the occurrence of the unstable creeping stage at the last stress level, the accumulated creep damage exceeded the damage limit of the composite sample, and the composite sample experienced the failure and instability.

(3) Under same stress level, with the increase of the stress level duration, the AE activities were strengthened. The intensity and frequency of AE events at different stages were enhanced. These illustrated that creep damage degree of the composite sample increased with the stress level duration under same stress level. These also can verify the accuracy of experimental results, i.e., the creep strength at a large stress level duration was smaller than that at a small stress level duration.

In order to better describe the creep damage evolution of the composite sample, the creep damage coefficient δ was defined as

$$\delta = \frac{A}{D} \quad (2)$$

where, A was cumulative count of AE events at creep stage for a stress level; D was creep time for a stress level. The values of δ of A-1 and B-3 composite samples under different stress levels are compared in Figure 15.

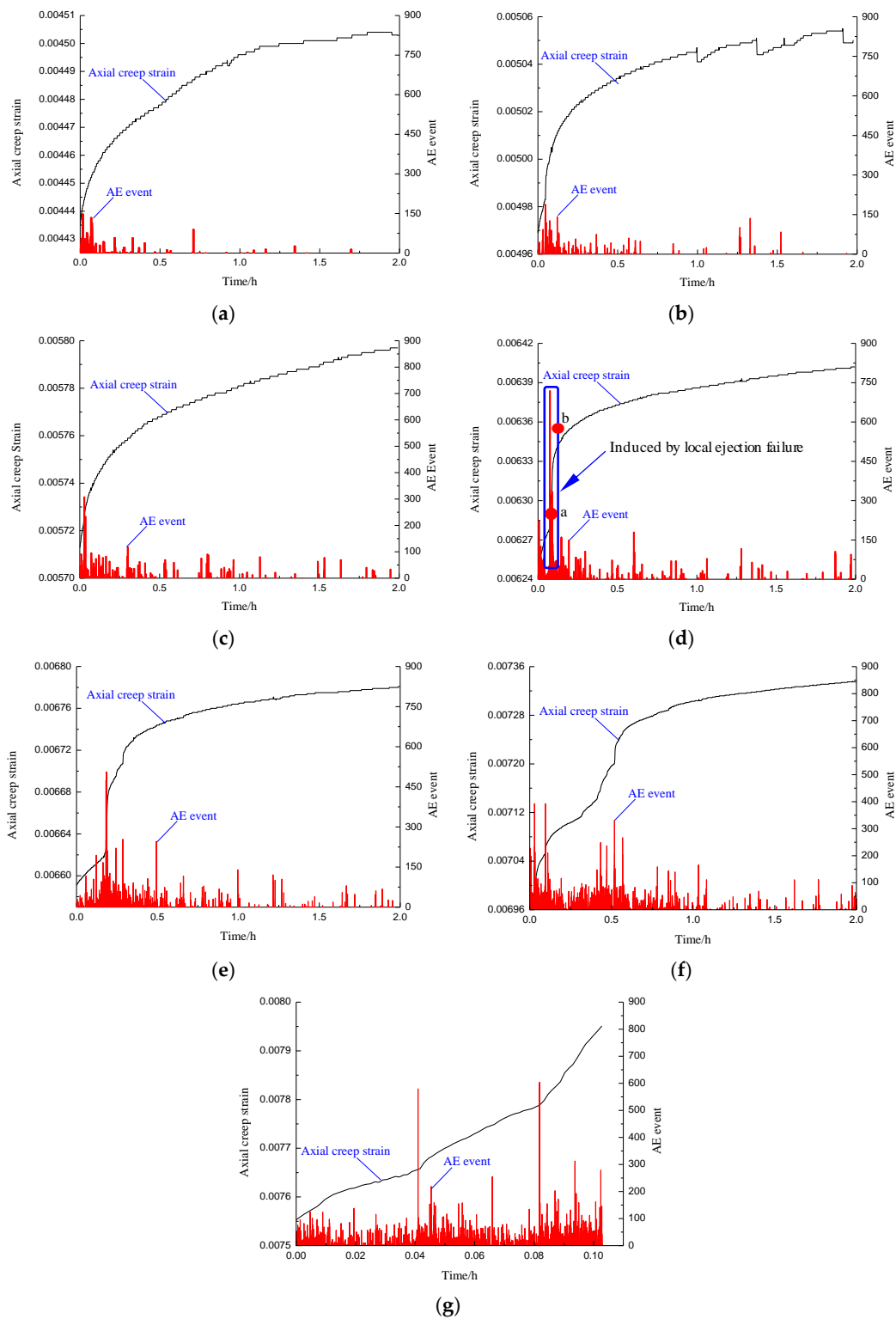


Figure 13. AE event variety curves of A-1 composite samples at creep stage for different stress levels: (a) AE event variety curve at the stress level of 7.07 MPa; (b) AE event variety curve at the stress level of 8.48 MPa; (c) AE event variety curve at the stress level of 9.90 MPa; (d) AE event variety curve at the stress level of 11.31 MPa; (e) AE event variety curve at the stress level of 12.02 MPa; (f) AE event variety curve at the stress level of 12.73 MPa; (g) AE event variety curve at the stress level of 13.44 MPa.

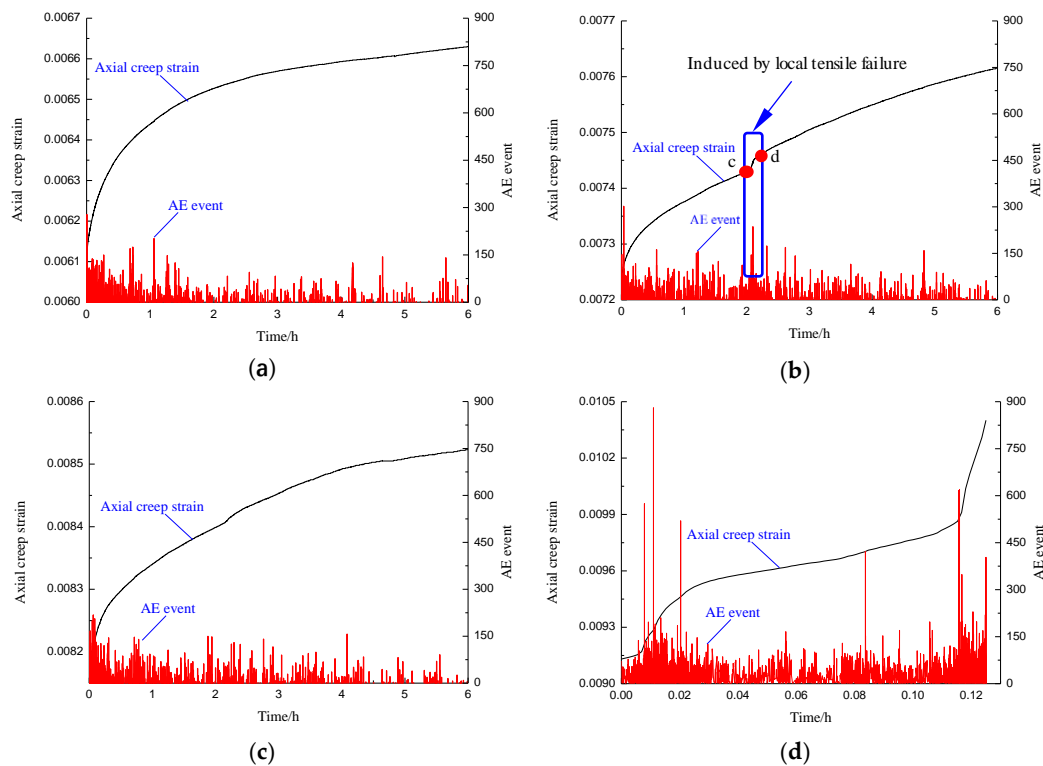


Figure 14. AE event variety curves of B-3 composite samples at creep stage for different stress levels: (a) AE event variety curve at the stress level of 7.07 MPa; (b) AE event variety curve at the stress level of 8.48 MPa; (c) AE event variety curve at the stress level of 9.90 MPa; (d) AE event variety curve at the stress level of 11.31 MPa.

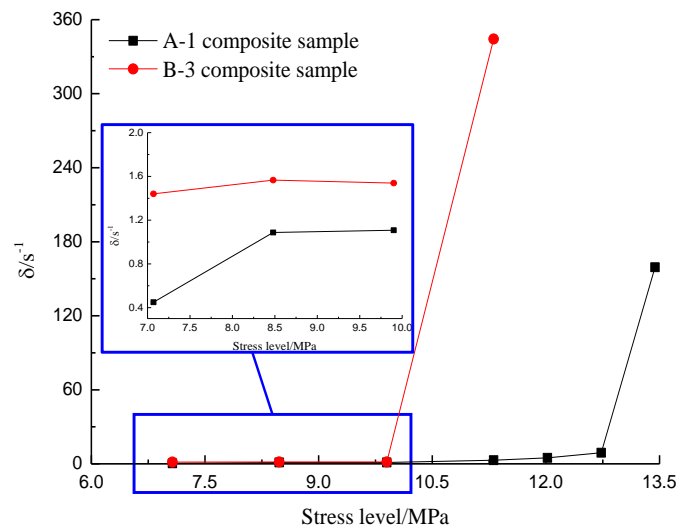


Figure 15. Comparison of δ values for A-1 and B-3 composite samples.

In Figure 15, under same stress level duration, δ increased with the stress level. These illustrated that the creep damage increased with the increase of the stress level. At the last stress level, δ showed a sharp increase with the most serious creep damage for the composite sample. Under same stress level, δ at a large stress level duration was greater than that at a small stress level duration. These illustrated that the creep damage of the composite sample at a large stress level duration was larger than that at a small stress level duration.

If the composite sample occurred the local failure or fracture at a stress level, the AE event would experience the peak value. For instance, the ejection failure of A-1 composite

sample caused the sudden increase of AE event at the stress level of 11.31 MPa, as shown in Figure 13d. And the AE event of B-3 composite sample experienced the relatively small peak value at the stress level of 8.48 MPa, as shown in Figure 14b.

6. Failure Characteristics of Composite Samples

6.1. Macro-Failure Patterns of Composite Samples

Figure 16a–f shows the macro-failure images of A-1, A-2, A-3, B-1, B-2, and B-3 composite samples under short-term uniaxial creep loading, respectively. In Figure 16, the failures of the composite samples mainly occurred within the coal, and no obvious failures were found in the sandstone. During creep loading, the coal experienced the ejection failure, ejecting small coal blocks. Further, the vertical tensile cracks were also found in the coal, as shown in red lines of Figure 16. Therefore, the coal mainly displayed the splitting ejection failure. With the increase of the stress level duration, the defects in the coal had sufficient time to propagate and coalesce, and the failure degrees of coal in Group B composite sample were greater than that in Group A composite samples.

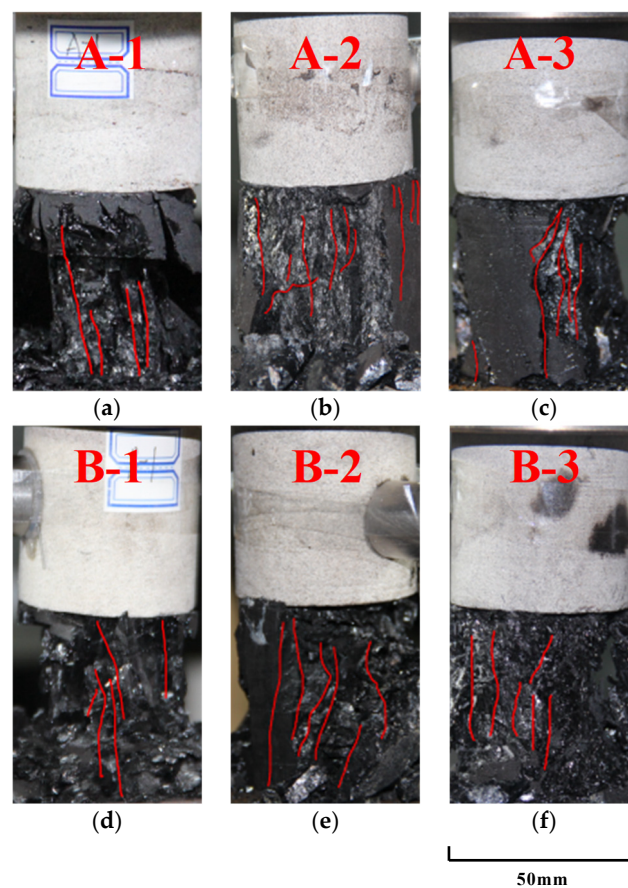


Figure 16. Macro-failure patterns of composite samples (the scale bar between the sample size in the figure and that of the real sample is 1:2): (a) Macro-failure pattern of A-1 composite sample; (b) Macro-failure pattern of A-2 composite sample; (c) Macro-failure pattern of A-3 composite sample; (d) Macro-failure pattern of B-1 composite sample; (e) Macro-failure pattern of B-2 composite sample; (f) Macro-failure pattern of B-3 composite sample.

6.2. Macro-Progressive Failure Characteristics

In the multi-step loading creep tests, the failure and instability of the composite sample were jointly caused by the creep damage due to the constant stress at each stress level, and by the loading damage between two adjacent stress levels as well as in the period from the initial loading point to the first stress level. These were attributed to the loading mechanism of our multi-step loading creep tests. The A-1 and B-3 composite samples were

selected to analyze the macro-progressive failure characteristics under different stress level durations, as shown in Figure 17I,II, respectively. Among them, the points of a~h represent the progressive failure points of the A-1 composite sample, and the points of i~o represent the progressive failure points of the B-3 composite sample.

In Figure 17I, there were two pre-existing vertical cracks on the surface of coal for A-1 composite sample. From the initial loading point to the second stress level (8.38 MPa), no obvious macro-failure was found on the surface of the composite sample, and the macro-failure occurred the deceleration creeping stage of the second stress level. Now, a small ejection failure (Blue ellipse in Figure 17I) occurred around the pre-existing vertical crack in coal accompanying by the tensile fracture. During the loading process from the second stress level to the third stress level (9.90 MPa), the composite sample experienced a relatively large failure. A tensile crack was first formed on the surface of coal, and then ejection failure occurred at the upper area of this crack, which was near the interface of sandstone and coal. Finally, the ejection failure zone could induce the chain destruction of the peripheral parts to form a large ejection failure zone along the tensile crack. At the deceleration creeping stage of the fourth stress level (11.31 MPa), the lower area of the large ejection failure zone experienced a small ejection failure again, and a small tensile fracture occurred in this area. When the axial stress reached 12.02 MPa (Fifth stress level), many macro-cracks were formed around the pre-existing vertical cracks and ejection failure zone, which were accompanied by small ejection failures. At the stable creeping stage of the stress level (12.73 MPa), more macro-cracks were generated on the surface of coal, and the ejection failure zones began to connect as a whole. At the last stress level (13.44 MPa), the propagation and coalescence of pre-existing vertical cracks and newborn macro-cracks made the coal become more broken, and a large ejection failure zone was formed on the surface of coal. Finally, these induced the failure of coal, and which further caused the whole instability and failure of the composite sample. Meanwhile, during this process, the rock rebound deformation enhanced the future failure of coal. Now, the composite sample lost the bearing capacity, and the axial stress decreased sharply with the rapid of axial strain.

In Figure 17II, the first macro-failure of B-3 composite sample occurred between the initial loading point and the first stress level (8.38 MPa). And a macro-tensile crack was formed on the surface of the coal. These indicated that the initial damage of coal was relatively large, and thus the creep strength of B-3 composite sample was comparatively small. There was no obvious macro-failure under the first stress level and between it and the second stress level (9.90 MPa). While, at the stable creeping stage of the second stress level, the coal displayed the tensile fracture, and a macro-tensile crack was found near the left area of the first macro-tensile crack. Between the second stress level and third stress level (11.31 MPa), more macro-tensile cracks were formed on the surface of the coal, and the lower part of the coal experienced a small ejection failure. At the stable creeping stage of the second stress level, the ejection failure zone induced the chain destruction of the peripheral parts to form a relatively large ejection failure zone in the coal, accompanied by the propagation and coalescence of macro-cracks. Then at the deceleration creeping stage of the fourth stress level (12.02 MPa), the composite sample occurred a large ejection failure. This caused the coal failure, and which then induced the whole instability and failure of the composite sample. Due to the large stress level duration, the rock rebound deformation was more serious, making the coal more broken than that of A-1 composite sample.

Meanwhile, when the composite experienced the macro-failure before final failure, a stress drop occurred on the stress-time curve. The axial stress decreased first and then increased, and this was the process from the failure to stability by adjusting the internal structures of the composite sample. The corresponding axial strain displayed fluctuations, and AE event occurred a peak value.

According to above analyses, the macro-failure of the composite sample occurred with the coal. The propagation and coalescence of pre-existing cracks and new-born cracks made the coal more broken, and the ejection failure zone induced the secondary ejection

failure of the peripheral parts to form a large ejection failure zone in the coal. These caused the final failure of coal, which resulted in the overall failure and instability of the composite sample. The rebound deformation of rock aggravates the fracture and movement of coal, promoting its failure degree, especially when the stress-level duration was large.

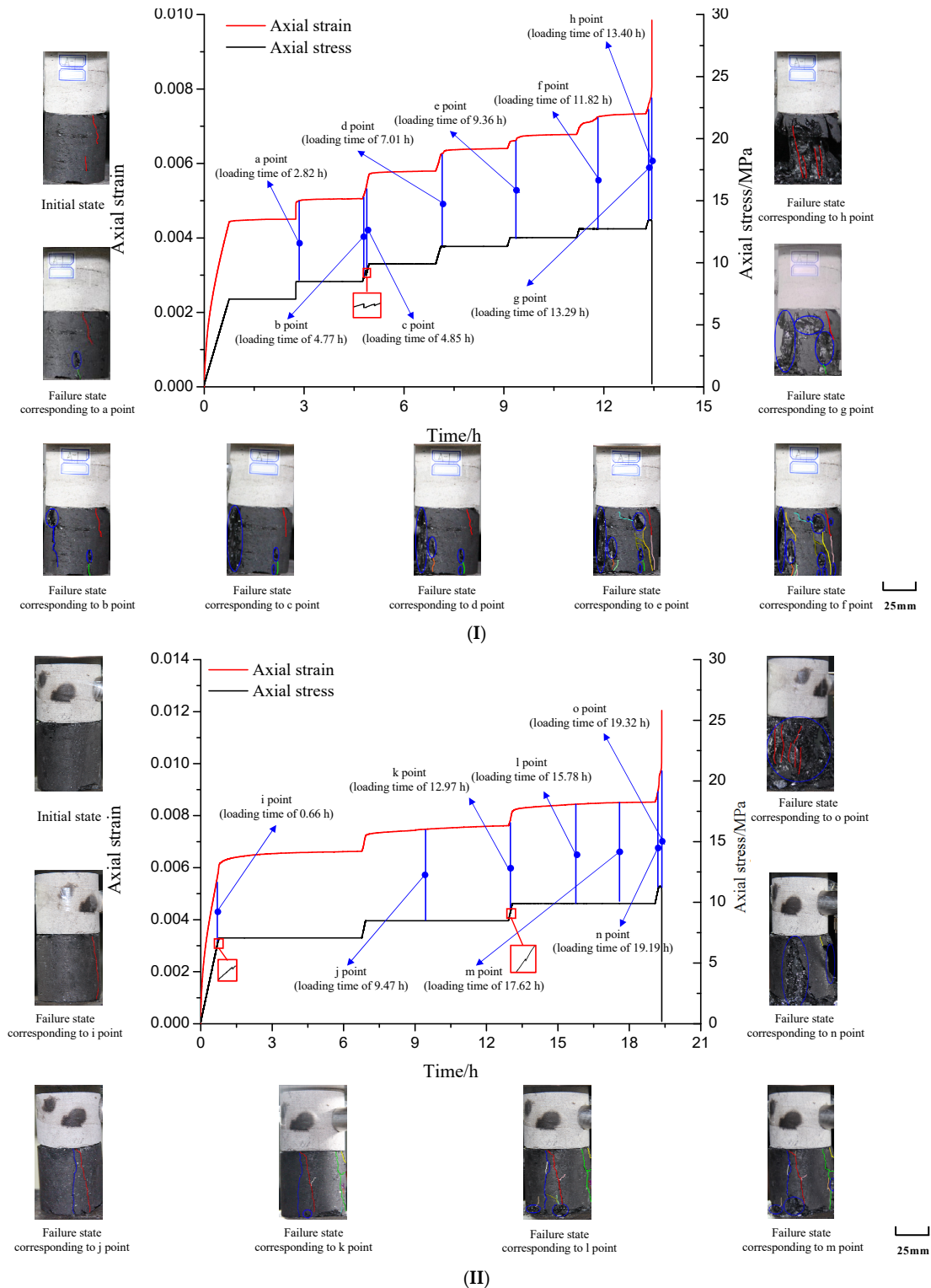


Figure 17. Macro-progressive failure processes of composite samples (the scale bar between the sample size in the figure and that of the real sample is 1:2.5): (I) Macro-progressive failure process of A-1 composite sample; (II) Macro-progressive failure process of B-3 composite sample.

7. Conclusions

In this paper, the uniaxial short-term multi-step loading creep tests with different stress-level durations were conducted on sandstone-coal composite samples to investigate their creep strengths, creep deformations, AE characteristics, and failure properties. The main conclusions are summarized as follows:

(1) The creep strength and creep coefficient of composite sample decreased with the stress-level duration. The average creep strength of Group A composite samples (stress level duration of 2 h) was 13.01 MPa with the average creep coefficient of 92.02%, and average creep strength of Group B composite samples (stress level duration of 6 h) was 11.39 MPa with the average creep coefficient of 80.55%. Compared with Group A composite samples, the average creep strength and creep coefficient of Group B composite samples both dropped by 12.45%. The creep strength of composite sample was mainly determined by the coal, which was influenced by the interactions with the sandstone. The creep deformation and damage within the sandstone induced by the stress levels reduced that within the coal, generally resulting in a higher creep strength for composite sample compared to pure coal sample.

(2) With the increase of the stress level, the axial creep strain of composite sample generally increased. Under same stress level, the larger the stress-level duration was, the greater the axial creep strain was. However, the micro failure or fracture and local macro failure or fracture within the composite sample caused the slight or sharp rise in axial creep strain, respectively.

(3) The AE characteristics of composite samples were related to the creep strain rate, stress level, stress level duration, and local failure or fracture within the composite sample, etc. Under same stress level, the frequency and intensity of AE signals were the most serious at the unstable creeping stage, and AE signals were the weakest at the stable creeping stage. While the frequency and intensity of AE signals at stages of deceleration creeping, stable creeping and unstable creeping increased with the increase of the stress level or stress level duration under same stress level duration or stress level. The local failure or fracture within the composite sample would enhance the AE activities, and the AE signals occurred peak values.

(4) The failures of the composite sample occurred with the coal, and no obvious failure was found in the sandstone. The propagation and coalescence of pre-existing cracks and new-born cracks made the coal more broken, and the ejection failure zone induced the secondary ejection failure of the peripheral parts to form a large ejection failure zone in the coal. These caused the final failure of coal, leading to the overall failure and instability of the composite sample. The rebound deformation of sandstone aggravates the fracture and movement of coal, promoting its failure degree, especially when the stress-level duration was large.

Author Contributions: Conceptualization, F.W.; methodology, F.W.; software, D.Y.; validation, J.Z., F.L. and C.Z.; data curation, J.Z.; writing—original draft preparation, D.Y.; writing—review and editing, D.Y. and F.F.; funding acquisition, F.W. All authors have read and agreed to the published version of the manuscript.

Funding: This work was supported by the National Science Foundation of China (51904167, 52074169), the Taishan Scholars Project, the Taishan Scholar Talent Team Support Plan for Advantaged & Unique Discipline Areas, the SDUST Research Fund, the Open Research Fund for the Key Laboratory of Safety and High-efficiency Coal Mining (JYBSYS2019201), the open funding of State Key Laboratory of Mining Disaster Prevention and Control Co-Founded by Shandong Province and The Ministry of Science and Technology (SICGM202104).

Data Availability Statement: The data are available and explained in this article; readers can access the data supporting the conclusions of this study.

Conflicts of Interest: The authors declare no conflict of interest.

References

1. Metallurgical Industry Energy Saving Committee of China Energy Saving Association. *China's Steel Industry Energy Saving and Low Carbon Development Report*; Metallurgical Industry Energy Saving Committee of China Energy Saving Association: Beijing, China, 2019. (In Chinese)
2. Gao, M.; Xie, J.; Gao, Y.; Wang, W.; Li, C.; Yang, B.; Liu, J.; Xie, H. Mechanical behavior of coal under different mining rates: A case study from laboratory experiments to field testing. *Int. J. Min. Sci. Technol.* **2021**, *31*, 825–841. [[CrossRef](#)]
3. Gao, M.; Xie, J.; Guo, J.; Lu, Y.; He, Z.; Li, C. Fractal evolution and connectivity characteristics of mining-induced crack networks in coal masses at different depths. *Géoméch. Geophys. Geo-Energy Geo-Resour.* **2021**, *7*, 1–15. [[CrossRef](#)]
4. Chen, S.; Yin, D.; Cao, F.; Liu, Y.; Ren, K. An overview of integrated surface subsidence-reducing technology in mining areas of China. *Nat. Hazards* **2016**, *81*, 1129–1145. [[CrossRef](#)]
5. Lama, R.; Bodziony, J. Management of outburst in underground coal mines. *Int. J. Coal Geol.* **1998**, *35*, 83–115. [[CrossRef](#)]
6. Cui, G.; Yang, L.; Fang, J.; Qiu, Z.; Wang, Y.; Ren, S. Geochemical reactions and their influence on petrophysical properties of ultra-low permeability oil reservoirs during water and CO₂ flooding. *J. Pet. Sci. Eng.* **2021**, *203*, 108672. [[CrossRef](#)]
7. Feng, G.R.; Bai, J.W.; Shi, D.X.; Qi, T.Y.; Wang, P.F.; Guo, J.; Wang, S.Y.; Kang, L.X. Key pillar theory in the chain failure of residual coal pillars and its application prospect. *J. China Coal Soc.* **2021**, *46*, 164–179. (In Chinese)
8. Bertuzzi, R.; Douglas, K.; Mostyn, G. An Approach to model the strength of coal pillars. *Int. J. Rock Mech. Min. Sci.* **2016**, *89*, 165–175. [[CrossRef](#)]
9. Chen, S.-J.; Guo, W.-J.; Zhou, H.; Shen, B.; Liu, J.-B. Field investigation of long-term bearing capacity of strip coal pillars. *Int. J. Rock Mech. Min. Sci.* **2014**, *70*, 109–114. [[CrossRef](#)]
10. Cui, G.; Wang, W.; Dou, B.; Liu, Y.; Tian, H.; Zheng, J.; Liu, Y. Geothermal Energy Exploitation and Power Generation via a Single Vertical Well Combined with Hydraulic Fracturing. *J. Energy Eng.* **2022**, *148*, 04021058. [[CrossRef](#)]
11. Salamon, M. Stability, instability and design of pillar workings. *Int. J. Rock Mech. Min. Sci. Géoméch. Abstr.* **1970**, *7*, 613–631. [[CrossRef](#)]
12. Salamon, M.D.G.; Ozbay, M.U.; Madden, B.J. Life and design of board-and-pillar workings affected by pillar scaling. *J. South. Afr. Inst. Min. Metall.* **1998**, *98*, 135–145.
13. Chen, S.J.; Yin, D.W.; Zhang, B.L.; Ma, H.F.; Liu, X.Q. Study on mechanical characteristics and progressive failure mechanism of roof-coal pillar structure body. *Chin. J. Rock Mech. Eng.* **2017**, *37*, 1588–1598. (In Chinese)
14. Yin, D.W.; Chen, S.J.; Xing, W.B.; Huang, D.M.; Liu, X.Q. Experimental study on mechanical behavior of roof-coal pillar structure body under different loading rates. *J. China Coal Soc.* **2018**, *43*, 1249–1257. (In Chinese)
15. Wang, T.; Jiang, Y.; Zhan, S.; Wang, C. Frictional sliding tests on combined coal-rock samples. *J. Rock Mech. Geotech. Eng.* **2014**, *6*, 280–286. [[CrossRef](#)]
16. Espinoza, D.N.; Pereira, J.-M.; Vandamme, M.; Dangla, P.; Vidal-Gilbert, S. Desorption-induced shear failure of coal bed seams during gas depletion. *Int. J. Coal Geol.* **2015**, *137*, 142–151. [[CrossRef](#)]
17. Zhao, T.-B.; Guo, W.-Y.; Lu, C.-P.; Zhao, G.-M. Failure characteristics of combined coal-rock with different interfacial angles. *Géoméch. Eng.* **2016**, *11*, 345–359. [[CrossRef](#)]
18. Li, W.; Bai, J.; Cheng, J.; Peng, S.; Liu, H. Determination of coal–rock interface strength by laboratory direct shear tests under constant normal load. *Int. J. Rock Mech. Min. Sci.* **2015**, *77*, 60–67. [[CrossRef](#)]
19. Yin, D.W.; Chen, S.J.; Liu, X.Q.; Ma, H.F. Effect of joint angle in coal on failure mechanical behavior of roof rock-coal combined body. *Q. J. Eng. Geol. Hydrogeol.* **2018**, *51*, 202–209. [[CrossRef](#)]
20. Yin, D.W.; Chen, S.J.; Ge, Y.; Liu, R. Mechanical properties of rockcoal bi-material samples with different lithologies under uniaxial loading. *J. Mater. Res. Technol.* **2021**, *10*, 322–338. [[CrossRef](#)]
21. Chen, S.J.; Yin, D.W.; Jiang, N.; Wang, F.; Guo, W.J. Simulation study on effects of loading rate on uniaxial compression failure of composite rock-coal layer. *Geomech. Eng.* **2019**, *17*, 333–342.
22. Yin, D.W.; Chen, S.J.; Sun, X.Z.; Jiang, N. Strength characteristics of roof rock-coal composite samples with different height ratios under uniaxial loading. *Arch. Min. Sci.* **2019**, *64*, 307–319.
23. Zhao, Z.; Lv, X.; Wang, W.; Tan, Y. Damage evolution of bi-body model composed of weakly cemented soft rock and coal considering different interface effect. *SpringerPlus* **2016**, *5*, 292. [[CrossRef](#)]
24. Zuo, J.P.; Chen, Y.; Zhang, J.W.; Wang, J.T.; Sun, Y.J. Failure behavior and strength characteristics of coal-rock combined body under different confining pressures. *J. China Coal. Soc.* **2016**, *41*, 2706–2713. (In Chinese)
25. Lu, J.; Huang, G.; Gao, H.; Li, X.; Zhang, D.; Yin, G. Mechanical Properties of Layered Composite Coal–Rock Subjected to True Triaxial Stress. *Rock Mech. Rock Eng.* **2020**, *53*, 4117–4138. [[CrossRef](#)]
26. Chen, S.J.; Yin, D.W.; Liu, H.M.; Chen, B.; Jiang, N. Effects of coal's initial macro-cracks on rockburst tendency of rock-coal bi-material samples. *R. Soc. Open Sci.* **2019**, *6*, 181795. [[CrossRef](#)]
27. Huang, B.X.; Liu, J.W. The effect of loading rate on the behavior of samples composed of coal and rock. *Int. J. Rock Mech. Min. Sci.* **2013**, *61*, 23–30. [[CrossRef](#)]
28. Nie, B.S.; He, X.Q.; Zhu, C.W. Study on mechanical property and electromagnetic emission during the fracture process of combined coal-rock. *Prog. Earth Planet. Sci.* **2009**, *1*, 281–287.
29. He, X.; Chen, W.; Nie, B.; Mitri, H. Electromagnetic emission theory and its application to dynamic phenomena in coal-rock. *Int. J. Rock Mech. Min. Sci.* **2011**, *48*, 1352–1358. [[CrossRef](#)]

30. Jin, P.; Wang, E.; Liu, X.; Huang, N.; Wang, S. Damage evolution law of coal-rock under uniaxial compression based on the electromagnetic radiation characteristics. *Int. J. Min. Sci. Technol.* **2013**, *23*, 213–219. [[CrossRef](#)]
31. Qu, X. *Experimental Study on Influence of Mechanical Properties of Roof and Floor on Stability of Strip Coal Pillar*; Shandong University of Science and Technology: Qingdao, China, 2018. (In Chinese)
32. Yin, D.W. *Experimental Study on Stabilities of Roof-Coal Pillar Structural Body*; Shandong University of Science and Technology: Qingdao, China, 2018. (In Chinese)
33. Guo, W.Y.; Tan, Y.L.; Yu, F.H.; Zhao, T.B.; Hu, S.C.; Huang, D.M.; Qin, Z. Mechanical behavior of rock-coal-rock specimens with different coal thicknesses. *Geomech. Eng.* **2108**, *15*, 1017–1027.
34. Zhang, H.; Wan, Z.; Zhang, Y.; Wu, D. Mechanical Properties and Failure Behavior of Composite Samples. *Adv. Mater. Sci. Eng.* **2018**, *2018*, 1–16. [[CrossRef](#)]
35. Zhang, H.; Elsworth, D.; Wan, Z. Failure response of composite rock-coal samples. *Géoméch. Geophys. Geo-Energy Geo-Resour.* **2018**, *4*, 175–192. [[CrossRef](#)]
36. Zhang, Z.T.; Liu, J.F.; Wang, L.; Yang, H.T.; Zuo, J.P. Effects of combination mode on mechanical properties and failure characteristics of the coal rock combinations. *J. China Coal Soc.* **2012**, *37*, 1677–1681. (In Chinese)
37. Fatemeh, S.R.; Mark, D.Z. Comparison of short-term and long-term creep experiments in shales and carbonates from unconventional gas reservoirs. *Rock Mech. Rock Eng.* **2018**, *51*, 1995–2014.
38. Cao, P.; Wen, Y.D.; Wang, Y.X.; Yuan, H.P.; Yuan, B. Study on nonlinear damage creep constitutive model for high-stress soft rock. *Environ. Earth Sci.* **2016**, *75*, 900. [[CrossRef](#)]
39. Maranini, E.; Brignoli, M. Creep behaviour of a weak rock: Experimental characterization. *Int. J. Rock Mech. Min. Sci.* **1999**, *36*, 127–138. [[CrossRef](#)]
40. Yang, S.-Q.; Jing, H.-W.; Cheng, L. Influences of pore pressure on short-term and creep mechanical behavior of red sandstone. *Eng. Geol.* **2014**, *179*, 10–23. [[CrossRef](#)]
41. Yang, D.; Chen, L.; Yang, S.; Chen, W.; Wu, G. Experimental investigation of the creep and damage behavior of Linyi red sandstone. *Int. J. Rock Mech. Min. Sci.* **2014**, *72*, 164–172. [[CrossRef](#)]
42. Zong, Y.; Han, L.; Jin, Y.; Zhao, W.; Meng, L. Experimental Investigation on the Post-Peak Short-Term and Creep Behavior of Fractured Sandstone. *Energies* **2020**, *13*, 598. [[CrossRef](#)]
43. Yang, Y.J.; Wang, D.C.; Zhao, N.N.; Chen, S.J. Acoustic emission characteristics of coal creep under step load. *J. Basic Sci. Eng.* **2013**, *21*, 159–166. (In Chinese)
44. Chen, S.J.; Guo, W.J.; Yang, Y.J. Experimental study of creep model and failure characteristics of coal. *Rock Soil Mech.* **2009**, *30*, 2595–2599. (In Chinese)
45. Cao, S.G.; Liu, Y.B.; Zhang, L.Q.; Jiang, Y.D. Experimental on acoustic emission of outburst-hazardous coal under uniaxial compression and creep. *J. China Coal Soc.* **2007**, *32*, 1264–1268. (In Chinese)
46. Wu, F.; Chen, J.; Zou, Q.L. A nonlinear creep damage model for salt rock. *Int. J. Damage Mech.* **2019**, *28*, 758–771. [[CrossRef](#)]
47. Wu, L.X.; Wang, J.Z. Preliminary exploration to rheology and micro-effect characteristics of coal. *Chin. J. Mech. Eng.* **1996**, *15*, 328–332. (In Chinese)